Available online at www.sciencedirect.com
SCIENCE DIRECT®
International Journal of Heat and Mass Transfer 47 (2004) 4761–4770
International Journal of HEAT and MASS TRANSFER
www.elsevier.com/locate/ijhmt

# Numerical study of a combined heat and mass recovery adsorption cooling cycle

K.C. Leong *, Y. Liu

*School of Mechanical and Production Engineering, Nanyang Technological University, 50 Nanyang Avenue, Singapore 639798, Singapore*

Received 22 December 2003; received in revised form 20 May 2004
Available online 21 July 2004

**Abstract**

A new transient two-dimensional model for the simulation of a combined heat and mass recovery adsorption cooling cycle based on the zeolite NaX/water working pair is proposed in this paper. The model describes the transfer phenomena in the adsorber in detail and is solved by control volume method. Internal and external mass transfer limitations which are neglected by many researchers are considered in the model since they have significant effects on the performance of the adsorption cooling cycle. The numerical results show that the combined heat and mass recovery cycle between two adsorbent beds can increase the coefficient of performance (COP) of an adsorption cooling system by more than 47% compared to the single bed cycle. This numerical model can be used in system optimization and design of adsorption cycles.


*Keywords:* Adsorption; Adsorbent; Cooling; Heat and mass recovery; Numerical model

## 1. Introduction

The most effective refrigerant, chlorofluorocarbons (CFCs), used in traditional vapor compression refrigeration systems are not environment friendly because they contribute to the depletion of the ozone layer and have a role in the greenhouse effect. Although other alternatives such as HCFCs and HFCs have less ozone layer depletion effect, they do have the potential of global warming. These environmental protection reasons intensify the research efforts on the development of both ozone layer and global warming safe refrigeration technology.

The environmental-friendly adsorption cooling system is an attractive alternative to the conventional vapor-compression cooling system. However, the widespread application of adsorption systems is limited by its rather low coefficient of performance (COP), low specific cooling power (SCP) and long cycle time. In order to improve the performances of the adsorption cooling system, some advanced cycles have been proposed and investigated, such as the continuous cycle [1], the forced convection cycle [2] and the thermal wave cycle [3]. The forced convection cycle and thermal wave cycle are both capable of achieving high COP values. However, these systems are inherently more complicated and are not suitable for actual engineering application. The continuous cycle which incorporates heat and mass recovery cycles is verified to be a simple and effective method to improve the thermal performance [4]. The function of

* Corresponding author. Tel.: +65 6790 4725/5596; fax: +65 6792 2619/4612.
*E-mail address:* mkcleong@ntu.edu.sg (K.C. Leong).

0017-9310/$ - see front matter © 2004 Elsevier Ltd. All rights reserved.
doi:10.1016/j.ijheatmasstransfer.2004.05.030

**Nomenclature**

| | |
|---|---|
| $C_p$ | specific heat ($J\,kg^{-1}\,K^{-1}$) |
| COP | coefficient of performance |
| $d$ | particle diameter (m) |
| $D_0$ | reference diffusivity ($m^2\,s^{-1}$) |
| $D_e$ | equivalent diffusivity in the adsorbent particles ($m^2\,s^{-1}$) |
| $D_g$ | diffusivity of water vapor ($m^2\,s^{-1}$) |
| $D_k$ | Knudsen diffusivity ($m^2\,s^{-1}$) |
| $D_m$ | molecular diffusivity ($m^2\,s^{-1}$) |
| $E_D$ | energy parameter in adsorption equilibrium equation (K) |
| $E_k$ | equivalent activation energy ($J\,mol^{-1}$) |
| $K$ | permeability of adsorbent bed ($m^2$) |
| $K_{ap}$ | apparent permeability ($m^2$) |
| $L$ | length of adsorbent bed (m) |
| $L_e$ | latent heat of vaporization ($J\,kg^{-1}$) |
| $m$ | mass (kg) |
| $M$ | molar mass ($kg\,mol^{-1}$) |
| $\boldsymbol{n}$ | normal vector of boundary surface |
| $P$ | pressure (Pa) |
| $q$ | adsorbed amount ($kg\,kg^{-1}$) |
| $r$ | radial coordinate (m) |
| $r_p$ | average pore diameter (m) |
| $R$ | universal gas constant ($J\,kmol^{-1}\,K^{-1}$); adsorber radius (m) |
| $S$ | boundary surfaces for adsorber |
| SCP | specific cooling power ($W\,kg^{-1}$) |
| $t$ | time (s) |
| $t_c$ | cycle time (s) |
| $t_h$ | heat recovery time (s) |
| $t_m$ | mass recovery time (s) |
| $T$ | temperature (K) |
| $u$ | vapor velocity in axial direction ($m\,s^{-1}$) |
| $u_f$ | fluid velocity ($m\,s^{-1}$) |
| $\bar{u}_f$ | average fluid velocity ($m\,s^{-1}$) |
| $\boldsymbol{u}$ | vapor velocity vector ($m\,s^{-1}$) |
| $v$ | vapor velocity in radial direction ($m\,s^{-1}$) |
| $z$ | axial direction (m) |

*Greek symbols*

| | |
|---|---|
| $\Delta H$ | heat of adsorption ($J\,kg^{-1}$) |
| $\varepsilon$ | total porosity |
| $\varepsilon_a$ | macro-porosity |
| $\varepsilon_i$ | micro-porosity |
| $\lambda$ | thermal conductivity ($W\,m^{-1}\,K^{-1}$) |
| $\mu$ | viscosity ($N\,s\,m^{-2}$ ) |
| $\rho$ | density ($kg\,m^{-3}$) |
| $\sigma$ | collision diameter for Lennard-Jones potential (Å) |
| $\tau$ | tortuosity |
| $\Omega$ | collision integral |

*Subscripts*

| | |
|---|---|
| a | adsorbed phase |
| a1 | begin of adsorption phase |
| a2 | end of adsorption phase |
| ap | apparent |
| c | condensing; cooling |
| e | evaporating |
| eq | equivalent |
| ev | evaporator |
| f | external heating exchange fluid |
| g | water vapor |
| g1 | begin of generation phase |
| g2 | end of generation phase |
| h | heating |
| in | inlet fluid |
| m | metal tube |
| s | adsorbent |

the heat recovery cycle is to recover the thermal energy from the temperature difference between the two adsorbent beds while mass recovery can increase the cycled refrigerant mass, which leads to improved performance. In order to achieve higher performance, mass recovery and heat regeneration can be simultaneously employed.

The thermodynamic investigation of a two-bed heat and mass recovery adsorption cycle has been carried out in recent years by several researchers [4–6]. Although they obtained some good results, their models gave only the COP values without any information of the transient heat and mass transfer. Numerical studies for intermittent cycle single bed systems with combined heat and mass transfer were performed by many investigators to predict the thermal performance of such systems [7–9]. However, these studies also did not take into account the transient heat and mass transfer processes in these advanced cycles. Poyelle et al. [10] proposed a simple one-dimensional numerical model for a heat and mass recovery adsorption-based air conditioning cycle. Mass transfer limitations were taken into account in their model. By assuming a parabolic pressure profile through the adsorbent bed, the average pressure inside the adsorbent was predicted. Although their model fitted the experiment data very well, there was a need to specify some empirical parameters a priori. This paper presents a two-dimensional heat and mass transfer model of a combined heat and mass recovery adsorption cycle.

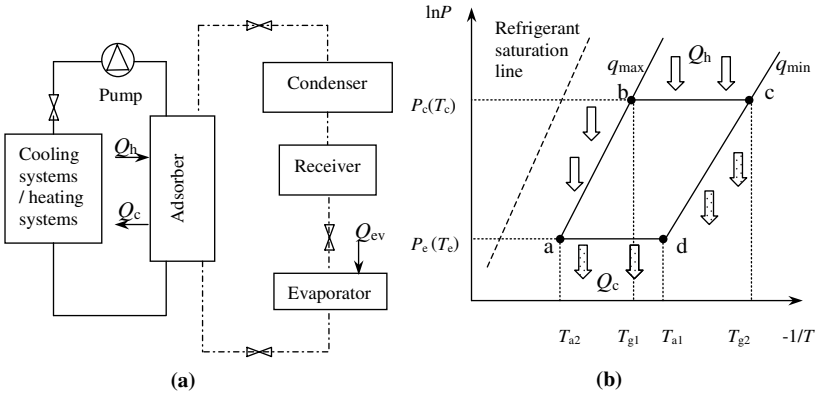


Fig. 1. A basic intermittent adsorption cooling cycle. (a) Schematic diagram, (b) Clapeyron diagram.

## 2. Background of adsorption cooling systems

The basic intermittent adsorption cooling cycle is composed of an adsorber alternately connected to a condenser and an evaporator (see Fig. 1(a)). The whole process consists of four phases. The Clapeyron diagram ($\ln P$ vs. $-1/T$) as shown in Fig. 1(b) can be used to analyze the operation of an adsorption heat transformer. During the first phase a–b, the adsorber containing a high concentration of adsorbate is heated at a constant adsorbed amount ($q_{max}$) from its initial temperature of $T_{a2}$ to a temperature $T_{g1}$. For the second phase b–c, the vapor pressure in the system is equal to the condensing pressure $P_c$ and desorption begins at $T_{g1}$ with the valve opened. The adsorbate desorbed from the adsorber is cooled to a temperature $T_c$ until it condenses in either a water or air-cooled condenser. During the first two phases, the external heat system provides an amount of heat $Q_h$. As the maximum temperature of the cycle is reached, the valve is closed and the adsorber is cooled down at a constant adsorbed amount ($q_{min}$) during the phase c–d. For the last phase d–a, the valve is opened and the adsorbate begins to evaporate from the evaporator and is adsorbed at constant pressure ($P_e$). During the last two phases, the adsorber will release heat with the amount of $Q_c$ to the external cooling systems. Two parameters, namely, the coefficient of performance (COP) and the specific cooling power (SCP) are used to assess the performance of a refrigerator. These are defined as follows:

$$\mathrm{COP} = \frac{Q_{ev}}{Q_h} \tag{1}$$

$$\mathrm{SCP} = \frac{Q_{ev}}{m_s \cdot t_c} \tag{2}$$

where $Q_{ev}$ is cooling production at the evaporator and is thus given by $Q_{ev} = m_s(q_{max} - q_{min})[L_e(T_e) - C_{pg}(T_c - T_e)]$, $m_s$ is the total mass of the adsorbent and $t_c$ is the time of adsorption cycle.

## 3. System description

The adsorption cooling system based on the zeolite NaX/water pair modeled in this paper is shown in Fig. 2. This system consists of six major components including two adsorbers, external heat and cooling systems, a condenser and an evaporator. Compared to the one-adsorber system, a two-adsorber cycle provides cooling on a more continuous basis (see Fig. 3). At the beginning of this two-bed cooling cycle, the adsorbent bed is at the state of point a and another bed is at the state of point c in Fig. 3. The mass recovery phase then starts. The two adsorbers are interconnected directly and the refrigerant vapor will flow from the high-pressure to the low-pressure adsorber. This process is maintained until the two

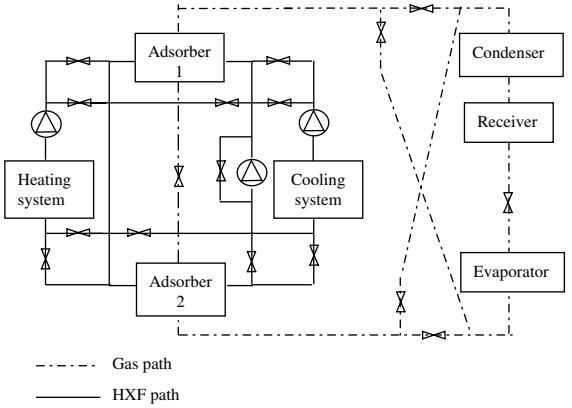


Fig. 2. Schematic diagram of two-bed adsorption refrigeration system with heat and mass recovery.

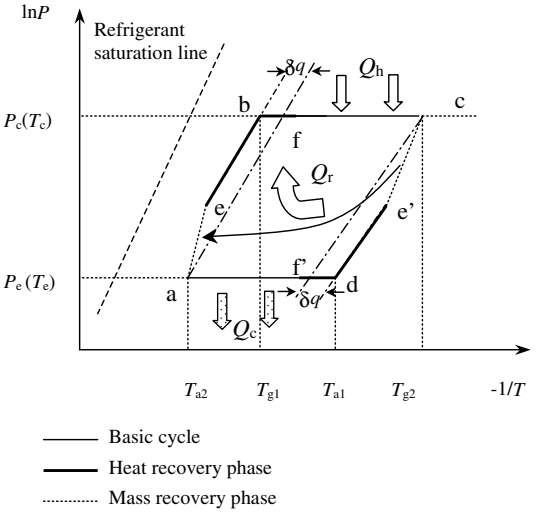


Fig. 3. Clapeyron diagram of combined heat and mass recovery cycle.

beds reach the same pressure (points e and e′) and the two adsorbers are disconnected. Subsequently, the heat recovery phase is carried out from point e to point f for adsorbent bed 1 and from point e′ to point f′ for the other bed. During this phase, no heat is supplied by the external heating systems and the amount of heat of $Q_r$ is exchanged between the two adsorbers. Finally the two adsorbent beds are connected to the external heating or cooling system, respectively. It can be seen in Fig. 3 that the cycle refrigerant mass will increase through the mass recovery cycle compared with the basic cycle, which leads to an increased value of $Q_{ev}$. Fig. 3 also shows that the amount of heat from external heat source $Q_h$ will decrease by using a heat recovery phase between the two adsorbers. Therefore, the COP will be increased for the combined heat and mass recovery cycle compared to the basic cycle (see Eq. (1)).

## 4. Mathematical modeling

A schematic of the adsorber is shown in Fig. 4. The adsorber is a hollow cylinder, which encloses a metal tube for the purpose of heat exchange between the solid adsorbent, and heating or cooling fluid within the tube. The adsorbate gas transfers heat to or from the adsorber.

The following assumptions are made:

(1) The adsorbed phase is considered as a liquid, and the adsorbate gas is assumed to be an ideal gas.
(2) The adsorbent bed is composed of uniform-size particles and has isotropic properties.
(3) The properties of the fluid, the metal tube and adsorbate vapor are constant.

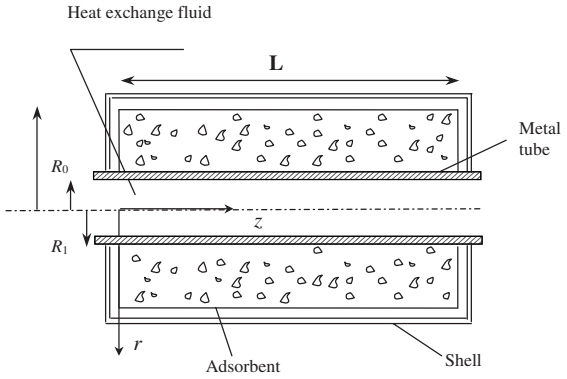


Fig. 4. Schematic diagram of adsorber.

(4) There are no heat losses in the adsorption cycle.
(5) The thermal resistance between the metal tube and the adsorbent bed is neglected. This is consistent with the findings of Zhu and Wang [11] who showed that the contact thermal resistance is equivalent to a 0.4 mm thick adsorbent used in our model.
(6) The flow of heat exchange fluid is assumed to be fully developed laminar flow. The velocity distribution is parabolic in the radial direction and remains constant in axial direction.

### 4.1. Adsorption equations

In most of the previous studies, the equilibrium adsorption model has been assumed and the mass transfer resistance between solid and adsorbate gas phase intra-particles is neglected. The LDF (linear driven force) model was used by Sakoda and Suzuki [12] to account for mass transfer resistance within the particles in a silica gel/water cooling cycle. Chahbani et al. [13] pointed out that the LDF model could be used to describe mass transfer resistance in the particles for a carbon/ammonia cycle. For an adsorption process in zeolite which follows the Langmuir-type isotherm, the LDF model can be used with about 15% error compared to the exact solution [14] when the adsorbed concentration is close to the equilibrium value. The adsorbent modeled in this paper is spherical zeolite NaX particles for which the LDF model is applicable. The model is described by

$$\frac{\partial \bar{q}}{\partial t} = \frac{15 D_e}{r_p^2}(q_{eq} - \bar{q}) \tag{3}$$

where $\bar{q}$ is the mean adsorbed concentration within the particle, and $q_{eq}$ is the adsorbed phase concentration in equilibrium with bulk fluid for zeolite NaX/water pair defined by the following equation containing three Langmuir terms [7]:

$$q_{eq} = \frac{q_{s,1} b_1 P}{1 + b_1 P} + \frac{q_{s,2} b_2 P}{1 + b_2 P} + \frac{q_{s,3} b_3 P}{1 + b_3 P} \tag{4}$$

where $q_{s,k}$ and $b_k$ ($k = 1$, 2, and 3) are functions of temperature as follows:

$$\begin{aligned} q_{s,k} &= a_{0,k} + \frac{a_{1,k}}{T_s} + \frac{a_{2,k}}{T_s^2} + \frac{a_{3,k}}{T_s^3} \quad (k = 1, 2) \\ q_{s,3} &= 0.267 - q_{s,1} - q_{s,2} \\ b_k &= b_{0,k} \exp(E_k / T_s) \end{aligned} \tag{5}$$

The values of the parameters in Eq. (5) are given in the literature [7].

$D_e$ is the equivalent diffusivity in the adsorbent particles which can be calculated by the following equation:

$$D_e = D_0 \exp(-E_D / RT_s) \tag{6}$$

where $D_0$ and $E_D$ can be obtained from experimental data available in the literature [15].

### 4.2. Energy conservation equations

The model describes the process, which is related to heat transfer between different components of the whole cooling system and mass transfer of refrigerant vapor in adsorber. The energy equations for different component of the two adsorbers can be developed as follows:

The energy balance on the thermal-fluid system yields:

$$\begin{aligned} &\frac{\partial(\rho_f C_{pf} T_f)}{\partial t} + \frac{u_f \partial(\rho_f C_{pf} T_f)}{\partial z} \\ &\quad = \frac{\partial}{\partial z}\left(\lambda_f \frac{\partial T_f}{\partial z}\right) + \frac{1}{r}\frac{\partial}{\partial r}\left(r\lambda_f \frac{\partial T_f}{\partial r}\right) \end{aligned} \tag{7}$$

The energy balance for the metal tube:

$$\frac{\partial(\rho_m C_{pm} T_m)}{\partial t} = \frac{\partial}{\partial z}\left(\lambda_m \frac{\partial T_m}{\partial z}\right) + \frac{1}{r}\frac{\partial}{\partial r}\left(r\lambda_m \frac{\partial T_m}{\partial r}\right) \tag{8}$$

The energy balance for the adsorbent:

$$\begin{aligned} &(\rho_s C_{ps} + \rho_s q C_{pa} + \varepsilon \rho_g C_{pg}) \frac{\partial T_s}{\partial t} + \frac{\partial(\rho_g C_{pg} u T_s)}{\partial z} \\ &\quad + \frac{1}{r}\frac{\partial}{\partial r}(r \rho_g C_{pg} v T_s) \\ &\quad = \frac{\partial}{\partial z}\left(\lambda_{eq} \frac{\partial T_s}{\partial z}\right) + \frac{1}{r}\frac{\partial}{\partial r}\left(r\lambda_{eq} \frac{\partial T_s}{\partial r}\right) + \rho_s \Delta H \frac{\partial \bar{q}}{\partial t} \end{aligned} \tag{9}$$

where subscripts f, m and s denote the heat exchange fluid, metal tube and adsorbent, respectively.

### 4.3. Mass conservation equations

The overall mass conservation in the adsorber is

$$\frac{\partial \varepsilon \rho_g}{\partial t} + \nabla \cdot (\rho_g \boldsymbol{u}) + \rho_s \frac{\partial \bar{q}}{\partial t} = 0 \tag{10}$$

and the water vapor velocity $\boldsymbol{u}$ can be defined by the Darcy's equation:

$$\boldsymbol{u} = -\frac{K_{ap}}{\mu} \nabla P \tag{11}$$

where $K_{ap}$ is the apparent permeability which can be obtained by considering the viscous flow and diffusion as follows [9]:

$$K_{ap} = K + \frac{\varepsilon_a \mu}{\tau P} D_g \tag{12}$$

The inherent permeability of the porous media, $K$, can be obtained from the semi-empirical Blake–Kozeny equation [16]:

$$K = \frac{\varepsilon_a^3 \times d^2}{150 \times (1 - \varepsilon_a)^2} \tag{13}$$

The diffusivity of water vapor, $D_g$ in Eq. (12) can be represented by the following equation [17]:

$$D_g = 1/(1/D_m + 1/D_k) \tag{14}$$

where

$$D_m = 0.02628 \frac{\sqrt{T^3/M}}{P\sigma^2 \Omega} \tag{15}$$

and

$$D_k = \frac{2 r_p}{3}\left(\frac{8RT}{\pi M}\right)^{1/2} = 97 r_p \left(\frac{T}{M}\right)^{1/2} \tag{16}$$

Substituting Eq. (11) into Eq. (10) for simplicity of calculation, we obtain

$$\frac{\partial\left(\frac{\varepsilon M}{RT} P\right)}{\partial t} = \frac{\partial}{\partial z}\left(\frac{\rho_g K_{ap}}{\mu}\frac{\partial P}{\partial z}\right) + \frac{1}{r}\frac{\partial}{\partial r}\left(\frac{r\rho_g K_{ap}}{\mu}\frac{\partial P}{\partial r}\right) - \rho_s \frac{\partial \bar{q}}{\partial t} \tag{17}$$

The initial and boundary conditions are listed below to complete the numerical formulation of the problem.

Initial conditions:

$$\begin{aligned} &\text{For } t = 0 \quad T_f(z,r) = T_{cin}; \\ &T_m(z,r) = T_s(z,r) = T_{a2}; \quad P = P_e \quad \text{(Adsorber 1)} \end{aligned} \tag{18}$$

$$\begin{aligned} &\text{For } t = 0 \quad T_f(z,r) = T_m(z,r) = T_s(z,r) = T_{g2}; \quad P = P_c \\ &\text{(Adsorber 2)} \end{aligned} \tag{19}$$

Boundary conditions:

$$\left.\frac{\partial T_f}{\partial z}\right|_{z=0} = \left.\frac{\partial T_f}{\partial z}\right|_{z=L} = 0$$

during mass recovery phase (20)

$$T_{f1}|_{z=0} = T_{f2}|_{z=L}; \quad T_{f2}|_{z=0} = T_{f1}|_{z=L}$$

during heat recovery phase (21)

$$T_f|_{z=0} = T_{hin}$$

when connected to external heating system (22)

$$T_f|_{z=0} = T_{cin}$$
when connected to external cooling system (23)

$$\left.\frac{\partial T_m}{\partial z}\right|_{z=0} = \left.\frac{\partial T_m}{\partial z}\right|_{z=L} = 0 \quad (24)$$

$$\left.\frac{\partial T_s}{\partial z}\right|_{z=0} = \left.\frac{\partial T_s}{\partial z}\right|_{z=L} = \left.\frac{\partial T_s}{\partial r}\right|_{r=R} = 0 \quad (25)$$

$$P_1|_{z=0} = P_1|_{z=L} = P_1|_{r=R} = P_a$$
during mass recovery phase for adsorber 1 (26)

$$P_2|_{z=0} = P_2|_{z=L} = P_2|_{r=R} = P_a$$
during mass recovery phase for adsorber 2 (27)

$$\left.\frac{\partial P}{\partial z}\right|_{z=0} = \left.\frac{\partial P}{\partial z}\right|_{z=L} = \left.\frac{\partial P}{\partial r}\right|_{r=R} = 0 \quad (28)$$

$$P|_{z=0} = P|_{z=L} = P|_{r=R} = P_e$$
when connected to evaporator (29)

$$P|_{z=0} = P|_{z=L} = P|_{r=R} = P_c$$
when connected to condenser (30)

where the symbols with subscripts 1 and 2 represent the properties of adsorber 1 and 2, respectively. Otherwise, these boundary conditions are suitable for the two adsorbers. $P_a$ is the pressure in the space between the adsorbent and the shell during mass recovery phase, and it is assumed to be equal for the two adsorbers during the mass recovery phase. During mass recovery phase, the water vapor will be transferred from adsorber 2 to adsorber 1, and the whole system is closed. Thus, the total mass flux for the system is zero and is presented as:

$$\oiint_{S1} \rho_g \boldsymbol{u} \cdot \boldsymbol{n}\,dS + \oiint_{S2} \rho_g \boldsymbol{u} \cdot \boldsymbol{n}\,dS = 0 \quad (31)$$

where $S1$ and $S2$ are the boundary surfaces for the two different adsorbers, respectively and $\boldsymbol{n}$ is the outward normal vector of the surface area. Substituting Darcy's equation into Eq. (31), we have

$$\oiint_{S1} \rho_g \frac{K_{ap}}{\mu} \nabla P \cdot \boldsymbol{n}\,dS + \oiint_{S2} \rho_g \frac{K_{ap}}{\mu} \nabla P \cdot \boldsymbol{n}\,dS = 0 \quad (32)$$

$P_a$ can be calculated from Eq. (32) by using an iteration technique.

## 5. Numerical method

The governing equations are solved by using the finite volume method described in detail by Patanker [18]. In the computational domain, a two-dimensional, non-uniform and staggered grid is used with a control volume formulation. The convection terms are discretized by using the power law scheme, the diffusion terms are discretized by the central difference scheme and the unsteady terms are discretized by the forward difference scheme. This algorithm provides a remarkably successful implicit method for simulating heat transfer in fluid flow. The discretized equations are solved by the line-by-line procedure, which is the combination of the Tri-Diagonal Matrix Algorithm (TDMA) and the Gauss–Seidel iteration technique.

Under-relaxation factors are employed to avoid divergence in the iterative solution of strongly nonlinear phenomena. The under-relaxation factors for the pressure and temperature are set to 0.5 and 0.8, respectively.

The influence of time step and grid size on the model results was analyzed to assess whether the time step and grid size employed are acceptable. A non-uniform mesh with a large concentration ranging from 10×40 to 30×100 grids and a time step ranging from 0.01 to 1 s was set up. The difference at different average temperature and pressure for 24×40 and 30×100 grids was found to be less than 5%. The difference at different average temperature and pressure between the 0.1 and 0.01 s time steps is less than 5%. Based on the analysis above, a time step between 0.01 and 0.1 s and 24× 40 grids were chosen to ensure the reliability of the results. The convergence criterion used in this method is $10^{-6}$.

## 6. Numerical results and discussion

A computer program was written based on the numerical methodology mentioned above to solve the model. Some parameters and operative conditions of the given base case used in the model are listed in the Table 1.

### 6.1. Analysis of mass recovery phase

The mass recovery phase is expected to accelerate the circulation and enhance the performance of the cycle. By using the mass recovery process, the quantity of refrigerant ($\Delta m$) in the evaporator is increased. The entire quantity of the cycled refrigerant can be written as:

$$\Delta m = m_s(q_{max} - q_{min}) = m_s \Delta q \quad (33)$$

where $\Delta q$ is the adsorbed amount change during the cooling cycle, which is given by $\Delta q = \Delta q_0 + \delta q$. $\delta q$ is the increase in adsorbed amount due to using mass recovery.

As mentioned in Section 3, the mass recovery phase starts with the connection with two adsorbers. The refrigerant vapor will be transferred from adsorber 2 to adsorber 1 because of the difference in pressure of the two adsorbers. This phase will end when the same pressure is obtained in the two adsorbers. The variations of the average pressure for both adsorbers with time are

Table 1
Parameter values and operating conditions used in the model

| Name | Symbol | Value |
|---|---|---|
| Average velocity of heating transfer fluid | $\bar{u}_f$ | 1 $ms^{-1}$ |
| Adsorption temperature | $T_{a2}$ | 318 K |
| Generation temperature | $T_{g2}$ | 473 K |
| Fluid inlet temperature during heating | $T_{hin}$ | 493 K |
| Fluid inlet temperature during cooling | $T_{cin}$ | 298 K |
| Evaporator temperature | $T_e$ | 279 K |
| Condenser temperature | $T_c$ | 318 K |
| Density of adsorbent | $\rho_s$ | 620 $kgm^{-3}$ |
| Specific heat of adsorbent | $C_{ps}$ | 836 $Jkg^{-1}K^{-1}$ |
| Thermal conductivity of adsorbent | $\lambda_s$ | 0.2 $Wm^{-1}K^{-1}$ |
| Heat of adsorption | $\Delta H$ | $3.2\times10^6$ $Jkg^{-1}$ |
| Particle diameter | $d$ | 0.2 mm |
| Internal radius of metal tube | $R_0$ | 0.020 m |
| External radius of metal tube | $R_1$ | 0.021 m |
| External radius of adsorbent bed | $R$ | 0.036 m |
| Length of adsorbent bed | $L$ | 0.60 m |
| Macro-porosity of adsorbent bed | $\varepsilon_a$ | 0.38 |
| Micro-porosity of adsorbent particle | $\varepsilon_i$ | 0.42 |
| Mass recovery time | $t_m$ | 55 s |
| Heat recovery time | $t_h$ | 2700 s |

shown in Fig. 5. From Fig. 5, the pressure in the low temperature adsorber (adsorber 1) increases to a maximum value in a very short time. At the same time, the pressure change in the high temperature adsorber (adsorber 2) is not as large. When the two adsorbers are connected, the refrigerant is transferred from adsorber 1 to adsorber 2. The mass of refrigerant vapor will increase rapidly and cannot be adsorbed in time in adsorber 1 because of intra-particle mass transfer limitation for adsorption process. This will lead to a rapid increase in the pressure. Compared with adsorber 1, adsorber 2 has higher diffusivity because of its higher temperature (see Eq. (6)). Thus, the intra-particle mass transfer resistance in adsorber 2 is smaller than that of adsorber 1 resulting in a lower pressure change in the high temperature adsorber. With increasing time, the refrigerant vapor will be adsorbed in the adsorbent and tends toward the equilibrium state with adsorbed phase. Therefore, the pressure will decrease slowly. Fig. 6 shows the variations of average adsorbed amount of the two adsorbers with time during the mass recovery phase. From Fig. 6, the adsorbed amount of adsorber 1 increases and adsorber 2 decreases with time during the mass recovery phase, and both the adsorbed amounts will tend to a constant value. It can also be seen that the adsorbed amount change for adsorber 1 is almost equal to that of adsorber 2. This also verifies the accuracy of the results because the entire system is closed and total mass flux is zero (Eq. (31)). The trend of pressure variation with time

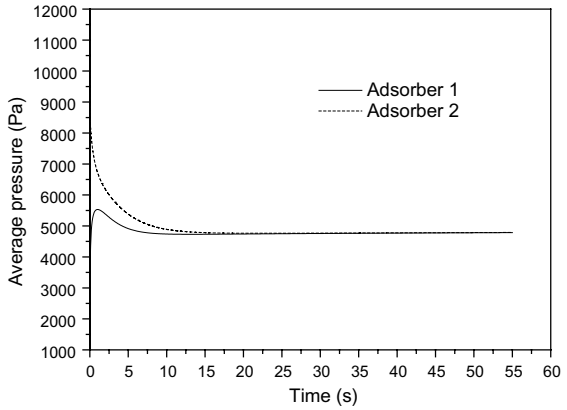


Fig. 5. Variation of average pressure with time during the mass recovery phase.

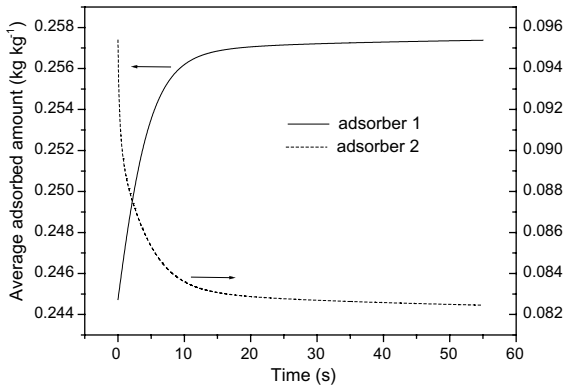


Fig. 6. Variation of average adsorbed amount with time during the mass recovery phase.

(Fig. 5) is very different from the trend of increase in adsorbed mass (Fig. 6) because of internal mass transfer limitation. The mass transfer process happens very quickly. The 99% adsorbed amount is completed in less than 35 s. This means that the performance can be improved by using a mass recovery phase without significant increase in the cycle time.

### 6.2. Results of combined heat and mass recovery cycle

In this section, the numerical simulation results of the adsorption cooling cycle with combined heat and mass recovery phase are presented.

The profiles of temperature, pressure and adsorbed amount of adsorbate with time are shown in Figs. 7–9. From Fig. 7, it can be seen that temperature increases rapidly during the mass recovery phase. The adsorption process carried out during the mass recovery phase and the adsorption heat released to adsorbent has caused the adsorbent temperature to increase. The same figure also shows that the slope of the heat recovery phase will lower than that of the basic cycle phase. For the heat recovery phase, the temperature gap between the two adsorbers is not high compared to the gap between the adsorber and external heat source or heat sink. The variation of pressure shown in Fig. 8 is similar to the ideal case. The pressure becomes a constant after a rapid and significant change for every half cycle. It can be deduced from Fig. 9 that the adsorbed amount will be almost a constant after mass recovery until the adsorber is connected to either the evaporator or condenser. The quantity of refrigerant vapor is also increased by the mass recovery phase as can be seen from the same figure.

Fig. 10 shows a comparison between a combined heat and mass recovery adsorption cycle and a basic cycle. It can be easily seen that the gap of the two isosteric lines is increased. See phases a–b and c–d in Fig. 1. This means

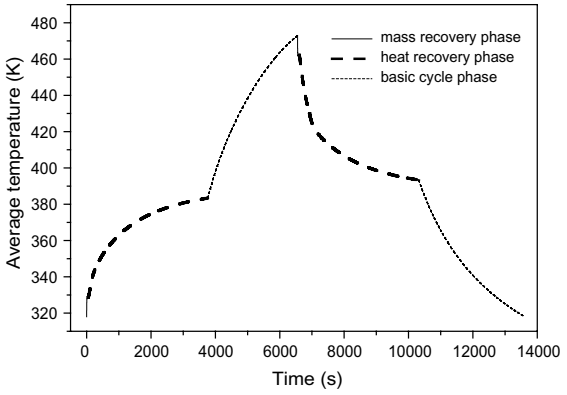


Fig. 7. Variation of average temperature with time for the whole cycle.

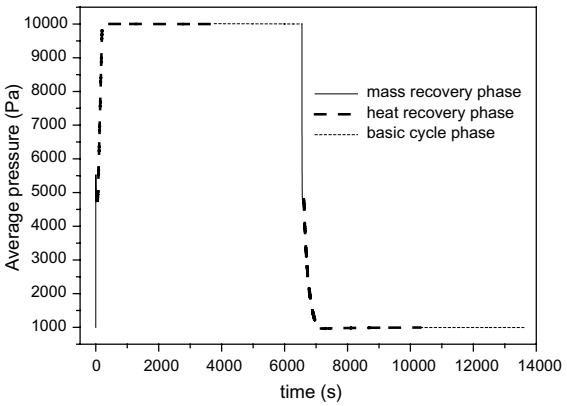


Fig. 8. Variation of average pressure with time for the whole cycle.

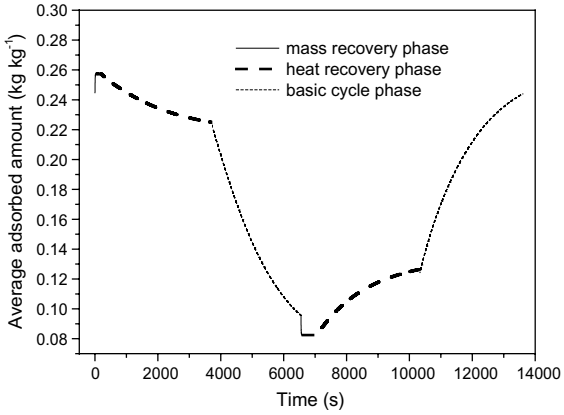


Fig. 9. Comparison of combined heat and mass recovery adsorption cycle and basic cycle.

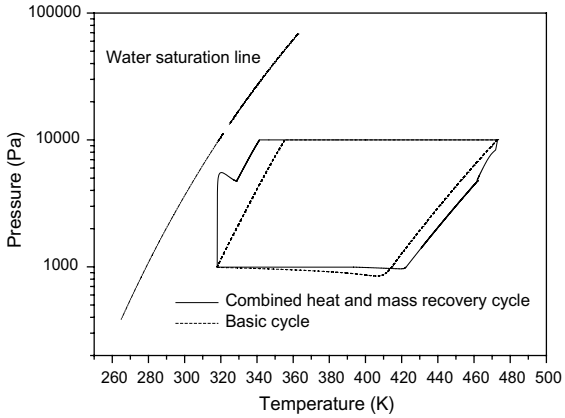


Fig. 10. Comparison of combined heat and mass recovery adsorption cycle and basic cycle.

that more refrigerant vapor is recycled compared with the basic cycle leading to an increase in cooling power produced. From Fig. 10, it can be seen that pressure is not a constant during the isobaric adsorption phase (see phase d–a in Fig. 1) for the basic cycle. Marletta et al. [9] suggested that this phenomenon may be the result of mass transfer limitation. However, for a cycle incorporating a combined heat and mass recovery phase, this phenomenon is not obvious. The effect of mass transfer limitation is reduced. When the adsorber is connected to the evaporator, the temperature gap between adsorber with HXF for heat and mass recovery cycle is smaller than that for a basic cycle. Hence, the mass flux of vapor from the evaporator to the adsorber of this advanced cycle is smaller than that of the basic cycle. Based on the same permeability, the pressure gradient in the adsorbent bed of this advanced cycle is also smaller than that of basic cycle. Thus, the average pressure in the heat and mass recovery cycle is closer to the ideal pressure.

### 6.3. Cycle performance

The main aim of using a combined heat and mass recovery cycle is to improve the system performance. Table 2 shows the calculated performance for different cycle types. It can be seen that for a cycle employing only mass recovery, the values of COP and SCP are both increased compared with the basic cycle. However, for a combined heat and mass recovery cycle, the significant increase in COP (by 47%) is accompanied by a reduction of about 40% in the SCP.

The results of the numerical simulation for the base case shown in Table 2 are compared with the results of Poyelle et al. [10]. For about the same operating temperature, the COP obtained in this study is 0.65, which is the same as that calculated by Poyelle et al. [10] without considering mass transfer resistance. Their experimental COP is 0.41, which is lower than the value obtained in our numerical study. This can be explained by the fact that the permeability ($10^{-13}\,m^2$) of the adsorbent bed in Poyelle et al's study is almost 5 times lower than the permeability used in our model. Their lower COP value is due to the larger mass transfer resistance of their adsorbent.

Since the mass recovery phase can be completed very quickly, the heat recovery time becomes a very important control parameter for performances. Fig. 11 shows

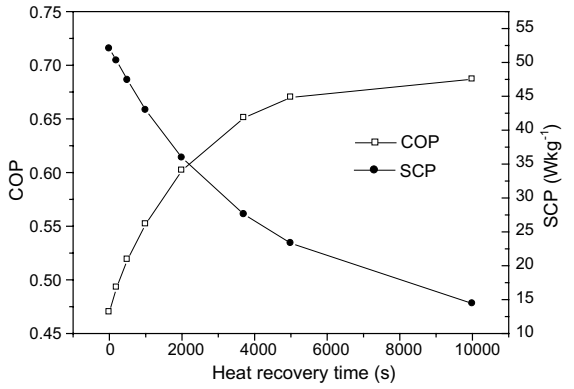


Fig. 11. Variation of performance parameters with the heat recovery time.

the effect of heat recovery time on the performances of an adsorption cycle employing heat and mass recovery. It can be seen that COP increases and tends to a constant value with an increase in heat recovery time. This is due to the decrease in $Q_h$ with an increase of heat recovery time. The temperature difference between the two adsorbers will becomes smaller compared with the temperature difference between the adsorber and external heat source. Hence, the heat exchange rate during the heat recovery phase is small compared to the basic cycle. The total cycle time will then increase with an increase in the heat recovery time leading to a penalty in terms of a reduction in SCP (see Fig. 12). Both the

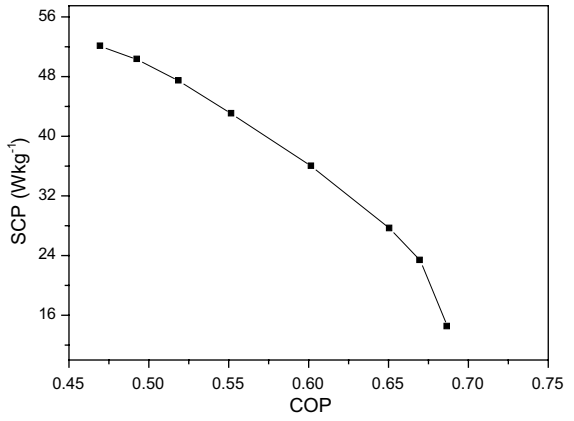


Fig. 12. Variation of the value of SCP with COP.

Table 2
Performances for different cycle types

| Cycle type | COP | SCP/W kg$^{-1}$ | Remarks |
|---|---|---|---|
| Basic cycle | 0.44 | 48.8 | $t_c = 7076$ s |
| Adsorption cycle with only mass recovery | 0.47 | 52.0 | $t_m = 55$ s |
| Adsorption cycle with combined heat and mass recovery | 0.65 | 27.6 | |

COP and SCP should be considered in the design of an adsorption cooling system. For different systems, the COP and SCP may be assigned different weights depending on their relative importance. For systems utilizing waste heat, the SCP is more important as the user is only concerned with the cooling power produced since the cost of producing the heat is almost zero. For other systems, the COP may be more important compared to SCP. Thus the selection of the operating conditions should consider the specific demands of the system.

## 7. Conclusion

A numerical transient model describing an adsorption refrigeration system based on the zeolite/water pair and incorporating a combined heat and mass recovery cycle is proposed in this paper. The resulting heat and mass transfer balance equations in two-dimensions are solved by the control volume method. The LDF equation is used to describe the micro mass transfer limitation in this model.

The mass recovery phase is very short (about 50 s) compared to the whole cycle time for the specified operating conditions. By using only the mass recovery cycle, the COP and SCP can be improved by about 6% and 7%, respectively compared to the basic cycle. The COP will increase and tend to a constant value while the SCP reduces with an increase in heat recovery time for the combined heat and mass recovery cycle. For the combined heat and mass recovery cycle with the given conditions, the calculated values of the COP and SCP are 0.651 and 27.58 $W\,kg^{-1}$, respectively. Although there is a significant increase in COP (by about 47%) compared to the basic cycle, there is an accompanied reduction in SCP by about 40%. Therefore, the selection of the operating conditions should consider the specific demands of the different systems.

## References

[1] G. Cacciola, G. Restuccia, Reversible adsorption heat pump: a thermodynamic model, International Journal of Refrigeration 18 (1995) 100–106.
[2] R.E. Critoph, Forced convection adsorption cycles, Applied Thermal Engineering 18 (1998) 799–807.
[3] D.J. Miles, Analysis and design of a solid adsorption heat driven heat pump, Ph.D. thesis, Georgia Institute of Technology, 1989.
[4] W. Wang, T.F. Qu, R.Z. Wang, Influence of degree of mass recovery and heat regeneration on adsorption refrigeration cycles, Energy Conversion and Management 43 (2002) 733–741.
[5] R.Z. Wang, Performance improvement of adsorption cooling by heat and mass recovery operation, International Journal of Refrigeration 24 (2001) 602–611.
[6] T.F. Qu, R.Z. Wang, W. Wang, Study on heat and mass recovery in adsorption refrigeration cycles, Applied Thermal Engineering 21 (2001) 439–452.
[7] N. Ben Amar, L.M. Sun, F. Meunier, Numerical analysis of adsorptive temperature wave refrigerative heat pump, Applied Thermal Engineering 16 (1996) 405–418.
[8] L.Z. Zhang, A three-dimensional non-equilibrium model for an intermittent adsorption cooling system, Solar energy 69 (2000) 27–35.
[9] L. Marletta, G. Maggio, A. Freni, M. Ingrasciotta, G. Restuccia, A non-uniform temperature non-uniform pressure dynamic model of heat and mass transfer in compact adsorbent beds, International Journal of Heat and Mass Transfer 45 (2002) 3321–3330.
[10] F. Poyelle, J.J. Guilleminot, F. Meunier, Experimental tests and predictive model of an adsorptive air conditioning unit, Industrial and Engineering Chemistry Research 38 (1999) 298–309.
[11] D. Zhu, S. Wang, Experimental investigation of contact resistance in adsorber of solar adsorption refrigeration, Solar Energy 73 (2002) 177–185.
[12] A. Sakoda, M. Suzuki, Fundamental study on solar power adsorption cooling system, Journal of Chemical Engineering of Japan 17 (1984) 52–57.
[13] M.H. Chahbani, J. Labidi, J. Paris, Effect of mass transfer kinetics on the performance of adsorptive heat pump systems, Applied Thermal Engineering 22 (2002) 23–40.
[14] R.T. Yang, Gas Separation by Adsorption Process, Butterworth, Stoneham, MA, 1987, pp. 128–129.
[15] Q. Wang, G. Chen, B. Han, The measurement of the equivalent diffusivity of adsorbent/adsorbent pair, Acta Energlae Solaris Sinica 22 (2001) 187–190.
[16] R.B. Bird, W.E. Stewart, E.N. Lightfoot, Transport Phenomena, Wiley, New York, 1960, pp. 181–207.
[17] M. Suzuki, Adsorption Engineering, Kodansha Ltd., Tokyo, 1990, pp. 63–93.
[18] S.V. Patankar, Numerical Heat Transfer and Fluid Flow, Hemisphere Publishing Corporation, New York, 1980.